Chinese Chemical Letters 32 (2021) 1759–1764

Contents lists available at ScienceDirect

Chinese Chemical Letters

journal homepage: www.elsevier.com/locate/cclet

Communication

# Ultrasound augmenting injectable chemotaxis hydrogel for articular cartilage repair in osteoarthritis

Hui Liu[a,b], Xi Xiang[a], Jianbo Huang[a], Bihui Zhu[a], Liyun Wang[a], Yuanjiao Tang[a], Fangxue Du[a], Ling Li[a], Feng Yan[a], Lang Ma[a,*], Li Qiu[a,*]

[a] Department of Ultrasound, Laboratory of Ultrasound Imaging Drug, West China Hospital, Sichuan University, Chengdu 610041, China
[b] Department of Ultrasound, The Affiliated Hospital of Southwest Medical University, Luzhou 646000, China

ARTICLE INFO

*Article history:*
Received 9 October 2020
Received in revised form 7 December 2020
Accepted 7 December 2020
Available online 11 December 2020

*Keywords:*
SDF-1$\alpha$
Injectable hydrogel
Ultrasound
Osteoarthritis
Cartilage repair

ABSTRACT

The increasing incidence of osteoarthritis (OA) seriously affects life quality, posing a huge socioeconomic burden. Tissue engineering technology has become a hot topic in articular cartilage repair as one of the key treatment methods to alleviate OA. Hydrogel, one of the most commonly used scaffold materials, can provide a good extracellular matrix microenvironment for seed cells such as bone marrow mesenchymal stem cells (BMSCs), which can promote cartilage regeneration. However, the low homing rate of stem cells severely limits their role in promoting articular cartilage regeneration. Stromal cell-derived factor-1$\alpha$ (SDF-1$\alpha$) plays a crucial role in the activation, mobilization, homing, and migration of MSCs. Herein, a novel injectable chemotaxis hydrogel, composed of chitosan-based injectable hydrogel and embedding SDF-1$\alpha$-loaded nanodroplets (PFP@NDs-PEG-SDF-1$\alpha$) was designed and fabricated. The ultrasound was then used to augment the injectable chemotaxis hydrogel and promote the homing migration of BMSCs for OA cartilage repair. The effect of ultrasound augmenting injectable PFP@NDs-PEG-SDF-1$\alpha$/hydrogel on the migration of BMSCs was verified *in vitro* and *in vivo*, which remarkably promotes stem cell homing and the repair of cartilage in the OA model. Therefore, the treatment strategy of ultrasound augmenting injectable chemotaxis hydrogel has a bright potential for OA articular cartilage repair.


Osteoarthritis (OA) is becoming more common and is one of the most common joint diseases, usually leading to progressive joint injury and irreversible joint degeneration. However, the inherent ability to repair adult cartilage after an injury is limited [1]. Traditional physiotherapy, drug therapy, and surgery can only provide relief of symptoms. Cell therapy [2,3] being used in cartilage repair continues to face prohibitive limitations because of their high costs and issues associated with cell treatment, time, and regulation related to patient safety [4]. Currently, there is no gold standard for cartilage repair [5]. Tissue engineering technology promotes the homing and differentiation of endogenous stem/progenitor cells [6], and combined with scaffold materials is a promising avenue for articular cartilage repair [7]. Tissue engineering includes three main elements, seed cells, scaffolds, and cytokines [8]. Stem cell therapy is becoming a potential strategy for tissue repair and regeneration in many medical fields [9]. Because of their self-renewal ability and multi-directional differentiation potential, MSCs can also enhance the host cartilage healing process through paracrine signaling [10,11]. Thus, MSCs therapy shows promising potential [12] to treat cartilage defects in patients with OA [13,14]. Among them, BMSCs are a better choice with high potential for seed cells.

Hydrogels have a variety of biological activities [15,16], such as improving the encapsulation and loading of drugs [17] and the unique potential in combination with nanoparticles [18]. Injectable thermosensitive hydrogel scaffolds have attracted considerable attention in heart, cartilage [19], bone, nerve tissue [20], and soft tissue regeneration [21]. They can be formed *in situ* and easily located to difficult-to-reach regions of the damaged cartilage, with less invasiveness [22]. Chitosan is the main compound of the extracellular matrix and as a cell scaffold can promote cartilage regeneration [23]. The stromal cell-derived factor 1 (SDF-1)/C-X-C chemokine receptor type 4 (CXCR4) signal axis plays an indispensable role in stem cell mobilization, migration, and homing [24]. Nevertheless, Stromal cell-derived factor 1$\alpha$ (SDF-1$\alpha$) is easily degraded when injected locally, making it problematic to control the dose and time of SDF-1$\alpha$ secretion. To improve the half-life of SDF-1$\alpha$ and its availability at the injection site, vectors [25–27] can be used for controlled and continuous release [28].

* Corresponding authors.
*E-mail addresses:* malang1989@scu.edu.cn (L. Ma), qiulihx@scu.edu.cn (L. Qiu).

https://doi.org/10.1016/j.cclet.2020.12.004
1001-8417/

Nanocarriers have been widely used in many fields [29–32]. Drug-loaded ultrasound contrast agent systems (URDDS) have become a hotspot of cartilage tissue engineering research [33]. Due to their small particle size, unique phase transition ability, good biocompatibility, and excellent tissue penetration, nanodroplets are commonly used carriers for the targeted delivery of drugs and genes and have been successfully applied to tissue engineering and the delivery of active cellular substances.

Herein, we design and fabricate a novel injectable chemotaxis hydrogel, composed of chitosan-based injectable hydrogel and embedding SDF-1$\alpha$-loaded nanodroplets (PFP@NDs-PEG-SDF-1$\alpha$). Ultrasounds were used to augment the injectable chemotaxis hydrogel and promote the homing migration of BMSCs for OA cartilage repair. The properties and structure of SDF-1$\alpha$-loaded nanodroplets were systematically studied *in vitro*, and the various physical and chemical properties of the hydrogels were analyzed. Besides, the cytotoxicity of injectable chemotaxis hydrogel was also evaluated. The effect of ultrasound augmenting injectable chemotaxis hydrogel on the migration of bone marrow mesenchymal stem cells (BMSCs) was verified by *in vitro* experiments. Finally, the ability of ultrasound augmenting injectable chemotaxis hydrogel to promote stem cell homing and cartilage repair was evaluated *in vivo* using an OA rat model. Based on histological and immunohistochemical analyses, ultrasound augmenting injectable chemotaxis hydrogel could be used to repair damaged cartilage tissue in the OA rat model. Our results suggest that the treatment strategy of ultrasound augmenting injectable chemotaxis hydrogel has a bright prospect when it is applied in OA articular cartilage repair.

Firstly, the SDF-1$\alpha$-loaded nanodroplets (PFP@-NDs-PEG-SDF-1$\alpha$) and the injectable chitosan hydrogel were prepared. Blank nanodroplets PFP@NDs-PEG were prepared by thin-film hydration and sonication as previously described [34]. The preparation and characterization of nanodroplets can be found in Supporting information. The schematic is shown in Figs. 1A and B. The average

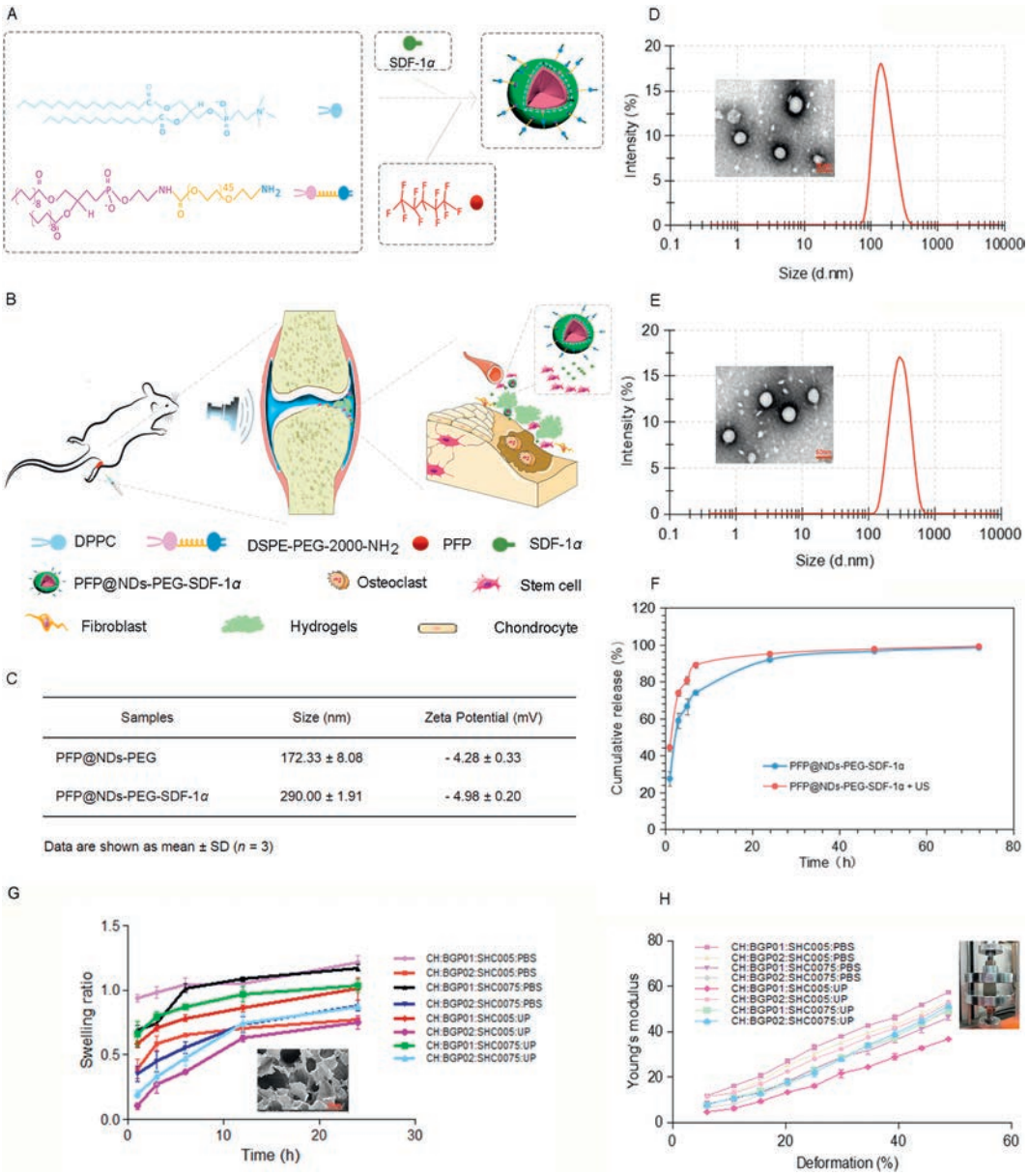


**Fig. 1.** Schematic of (A) the synthesis of PFP@NDs-PEG-SDF-1$\alpha$ and (B) the process of *in vivo* treatment with ultrasound. (C) The average size and zeta potential of the nanodroplets. Size distribution and TEM images of (D) blank PFP@NDs-PEG, (E) PFP@NDs-PEG-SDF-1$\alpha$. Scale bars: 50 nm. (F) SDF-1$\alpha$ release curves for PFP@NDs-PEG-SDF-1$\alpha$ with or without the US in PBS (pH 7.4) at 37 °C ($n$ = 3). (G) The swelling curve of each hydrogel within 24 h, SEM images of CH:BGP02:SHC0075:UP group chitosan hydrogels at 50×. (H) Strain-stress curves obtained by unconfined compressive mechanical tests.

sizes of PFP@NDs-PEG and PFP@NDs-PEG-SDF-1$\alpha$ nanodroplets were $172.33 \pm 8.08$ and $290.00 \pm 1.91$ nm, respectively (Fig. 1C). The results demonstrated that the coupling of SDF-1$\alpha$ affected the size distribution of hydrated particles. Besides, the average zeta potentials of blank PFP@NDs-PEG and PFP@NDs-PEG-SDF-1$\alpha$ nanodroplets were negative charges of $-4.28 \pm 0.33$ mV and $-4.89 \pm 0.20$ mV, respectively. The negatively charged surfaces made the nanodroplets more stable. The zeta potential and particle size of the nanodroplets made it easy to produce the enhanced permeability and retention (EPR) effect, which indicates they can effectively penetrate tissue. TEM images (Figs. 1D and E) showed the nanoparticles were monodispersed and spherical. The EE of SDF-1$\alpha$ in the PFP@NDs-PEG-SDF-1$\alpha$ nanodroplets was 95.62% $\pm$ 0.02% and the DL was 2.049 μg/mg. The hemolysis rates were 1.50% $\pm$ 0.14% for PFP@NDs-PEG and 1.43% $\pm$ 0.06% for PFP@NDs-PEG-SDF-1$\alpha$. The results showed that intravenous injection of PFP@NDs-PEG-SDF-1$\alpha$ is very safe. The nanodroplets exhibited good stability at low temperatures, indicating that the lipid shell provided a good protective effect and suggested great potential for nanodroplets to be used as carriers *in vivo*. There was a significant difference in the cumulative release rate between groups with and without ultrasound treatment (Fig. 1F). During the first 48 h, there was a significant difference in the cumulative release rate between groups with and without ultrasound treatment. The release curve of SDF-1$\alpha$ *in vitro* showed that ultrasound could promote and accelerate the release of chemokines from nanodroplets.

The preparation and characterization methods of hydrogels can be found in the supplementary material. $\beta$-Glycerophosphate pentahydrate (BGP) and sodium hydrogen carbonate (SHC) was dissolved in ultrapure (UP) water or PBS (pH 7.4). BGP:SHC:PBS and BGP:SHC:UP solutions were prepared at different ratios of SHC and BGP and were used as the gel solutions. Then the chitosan (CH) solution was combined with the gel solution, the final CH concentration of all hydrogels was 2% (w/v) (Table S1 in Supporting information). Simply, the injectable chitosan thermosensitive hydrogel is referred to as hydrogel in the subsequent sections of this work. The pH of all hydrogel samples was between 6.9 and 7.3, and gel time was 1 min for all hydrogels except CH:BGP01:SHC005:PBS, which had a gel time of 3 min (Table S2 in Supporting information). Thus, all hydrogels could gel in a relatively short amount of time.

SEM images of the freeze-dried hydrogel samples reveal homogeneous pores with interconnected pores. All freeze-dried hydrogel samples show irregular porous morphology (Fig. S1A in Supporting information). The use of additional $NaHCO_3$ may be more conducive to cell growth as a rough bottom [35] usually enhances the initial attachment of cells [36]. The hydrogel swelling characteristics were shown in Fig. 1G [37]. The Swelling Rate (SR) values of each hydrogel are measured that all the hydrogels exhibit slightly higher SR values (Fig. S1B in Supporting information). Lower concentrations of BGP result in higher swelling ability. Swelling characteristics and structural stability are two important parameters that should be considered to apply hydrogels and scaffolds in tissue engineering. The Young's modulus (Fig. 1H) increased with deformation reflects the typical nonlinear behavior of hydrogels. All hydrogels show slightly higher Young's modulus because of sodium bicarbonate. The Young's modulus for the PBS groups of hydrogels is higher relative to that of the pure water group. The infrared spectrum (Fig. S1C in Supporting information) shows the characteristic absorption bands of these polymers. The results can be found in Supporting information.

The procedure and some of the results of the *in vitro* experiment can be found in the supplementary material. The identification of BMSCs is confirmed by flow cytometry and osteogenic and lipogenic induction (Fig. S2 in Supporting information). Based on comprehensive analyses, CH:BGP02:SHC0075:UP hydrogels are selected for *in vitro* and *in vivo* experiments as they have a suitable elastic modulus. The nanodroplets and hydrogels exhibit no obvious cytotoxicity (Fig. S3 in Supporting information). Transwell migration assays are used to assess the ability of SDF-1$\alpha$ to induce BMSCs migration. The migration efficiency of BMSCs increases with PFP@NDs-PEG-SDF-1$\alpha$ concentrations from 0 to 200 ng/mL (Figs. S4A and S4C in Supporting information), which may be related to cell migration caused by the SDF-1-CXCR4 axis. There is no significant difference in the migration efficiency of BMSCs at 200 ng/mL and 400 ng/mL PFP@NDs-PEG-SDF-1$\alpha$ ($P > 0.05$). Therefore, the PFP@NDs-PEG-SDF-1$\alpha$ group at a 200 ng/mL concentration is selected for follow-up experiments. Using the same methodology, different experimental conditions for the lower chamber are applied according to the different groups. Specifically, there were seven groups in the current study, including (a) the control group, (b) the SDF-1$\alpha$ group, (c) the SDF-1$\alpha$ group + AMD3100 group, (d) the PFP@NDs-PEG-SDF-1$\alpha$ group, (e) the PFP@NDs-PEG-SDF-1$\alpha$ + ultrasound (ultrasound, US) group, (f) the PFP@NDs-PEG-SDF-1$\alpha$/hydrogel group, and (g) the PFP@NDs-PEG-SDF-1$\alpha$/hydrogel + US group. The number (Fig. S4B and S4D in Supporting information) of BMSCs migrations for the control group, AMD3100 group, and hydrogel group is lower than the other groups. However, the number of BMSCs migrations is significantly increased in the SDF-1$\alpha$ group, PFP@NDs-PEG-SDF-1$\alpha$ group, PFP@NDs-PEG-SDF-1$\alpha$ + US group, PFP@NDs-PEG-SDF-1$\alpha$/hydrogel group, and PFP@NDs-PEG-SDF-1$\alpha$/hydrogel + US group compared to the control group. *In vitro* cell migration assays reveal that SDF-1$\alpha$ has an obvious migration effect on BMSCs. At the same SDF-1$\alpha$ concentrations, migration is significantly enhanced with SDF-1$\alpha$ compared to that of the control group, which indicates that the biological activity of SDF-1$\alpha$ is not affected by the nanodroplets or ultrasound irradiation and still has chemotactic effects on stem cells.

*In vivo* experiments include ultrasound combined with PFP@NDs-PEG-SDF-1$\alpha$/hydrogel induced homing of stem cells and ultrasonic combined with PFP@NDs-PEG-SDF-1$\alpha$/hydrogel for articular cartilage regeneration. The procedure and some of the results of the *in vivo* experiment can be found in the supplementary material. The bilateral knee OA model was established using the modified Hulth model previously described [38]. Six weeks after the operation, the rats were then randomly divided into seven experimental groups ($n = 6$), including (a) the control group, (b) the PFP@NDs-PEG-SDF-1$\alpha$/hydrogel group, (c) the PFP@NDs-PEG-SDF-1$\alpha$/hydrogel + US group, (d) the PFP@NDs-PEG-SDF-1$\alpha$ intravenous (intravenous, i.v.) group, (e) the PFP@NDs-PEG-SDF-1$\alpha$ (i.v.) + US group, (f) the PFP@NDs-PEG-SDF-1$\alpha$ (i.v.) + PFP@NDs-PEG-SDF-1$\alpha$/hydrogel group, and (g) the PFP@NDs-PEG-SDF-1$\alpha$ (i.v.) + PFP@NDs-PEG-SDF-1$\alpha$/hydrogel + US group. *In vivo* homing of stem cells (Fig. 2), we found that the number of cells expressing CD44 and CD29 in the PFP@NDs-PEG-SDF-1$\alpha$ (i.v.) + PFP@NDs-PEG-SDF-1$\alpha$/hydrogel + US group is higher than that in other groups, and these cells did not express CD45. Furthermore, PFP@NDs-PEG-SDF-1$\alpha$ can enhance cell membrane permeability under ultrasonic irradiation and enhance cell uptake through cavitation when exposed to ultrasound. Similarly, ultrasound increased passive targeting through the EPR effect and released more chemokines by disrupting the nanodroplets. Ultrasound increases exosmosis and the internalization of carriers and chemokines and increases chemokine diffusion in tissues, thereby improving stem cell homing efficiency [39]. Blood vessels in a lesion area are more prone to leakage, resulting in a larger window between endothelial cells and damaged lymphoid reflux, leading to enhanced extravasation and retention of nanoscale ultrasound contrast agents [40,41]. The EPR effect plays a key role in the passive targeting of nanodroplets. Inflammatory capillary leakage brings nanocarriers into the inflamed joint [42].

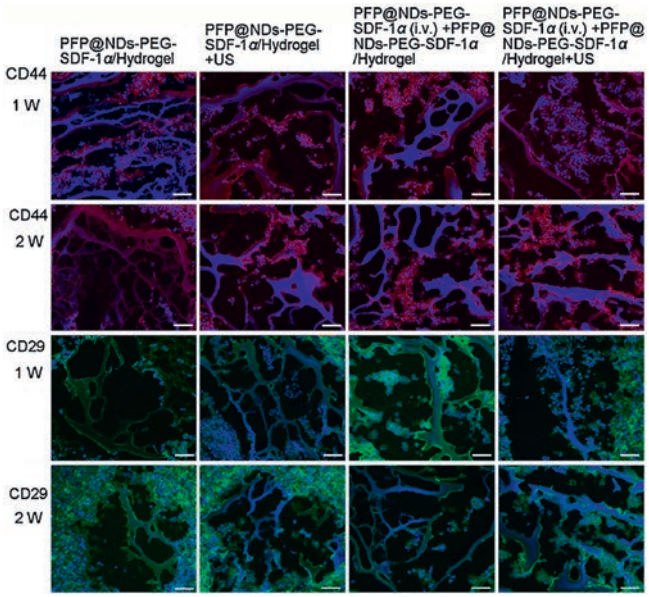


**Fig. 2.** Immunostaining for surface antigens CD44 and CD29 was used to identify stem cells in each group's hydrogels. Scale bar: 50 μm.

Pathological examinations were performed 6 and 12 weeks after OA treatment. The joint tissues were stained with H&E, SO/FG, and Masson's trichrome staining (Fig. 3). Immunohistochemical examination of type I and type II collagen were also performed in each group after treatment at the same time (Fig. 4). Results of H&E, SO/FG, Masson's trichrome staining, expression level of type I collagen and type II collagen, intergroup comparisons can be found in the supplementary material. H&E staining indicates that the cartilage surfaces of the control group and PFP@NDs-PEG-SDF-1$\alpha$ (i.v.) group are poorly repaired, which is especially true for the cartilage surface of the PFP@NDs-PEG-SDF-1$\alpha$ (i.v.) + PFP@NDs-PEG-SDF-1$\alpha$/Hydrogel + US group that is the smoothest among all the groups. The Osteoarthritis Research Society International (OARSI) scores [43] (Fig. S5A in Supporting information) of the control group and PFP@NDs-PEG-SDF-1$\alpha$ (i.v.) group are higher than those of the other groups, while the OARSI score in the PFP@NDs-PEG-SDF-1$\alpha$ (iv) + PFP@NDs-PEG-SDF-1$\alpha$/hydrogel + US group is the lowest, indicating the best cartilage repair effect. Proteoglycan is an extracellular matrix component necessary for cartilage repair and is vital for normal cartilage regeneration [44,45]. SO/FG showed proteoglycan deficiency in the control group. The contents of other histone polysaccharides are all increased to different degrees, especially in the PFP@NDs-PEG-SDF-1$\alpha$ (i.v.) + PFP@NDs-PEG-SDF-1$\alpha$/hydrogel + US group, which has better cartilage matrix tissue and higher content of proteoglycan. Masson's trichrome staining shows that the control group and PFP@NDs-PEG-SDF-1$\alpha$ (i.v.) group have superficial and intermediate cartilage neoplasia with a muscle fiber formation matrix. In contrast, the other groups have only a small amount of muscle fiber matrix formed in the deep cartilage layer. Based on immunohistochemical detection of type I and type II collagen expression (Figs. S5B and S5C in Supporting information), the collagen content in the PFP@NDs-PEG-SDF-1$\alpha$

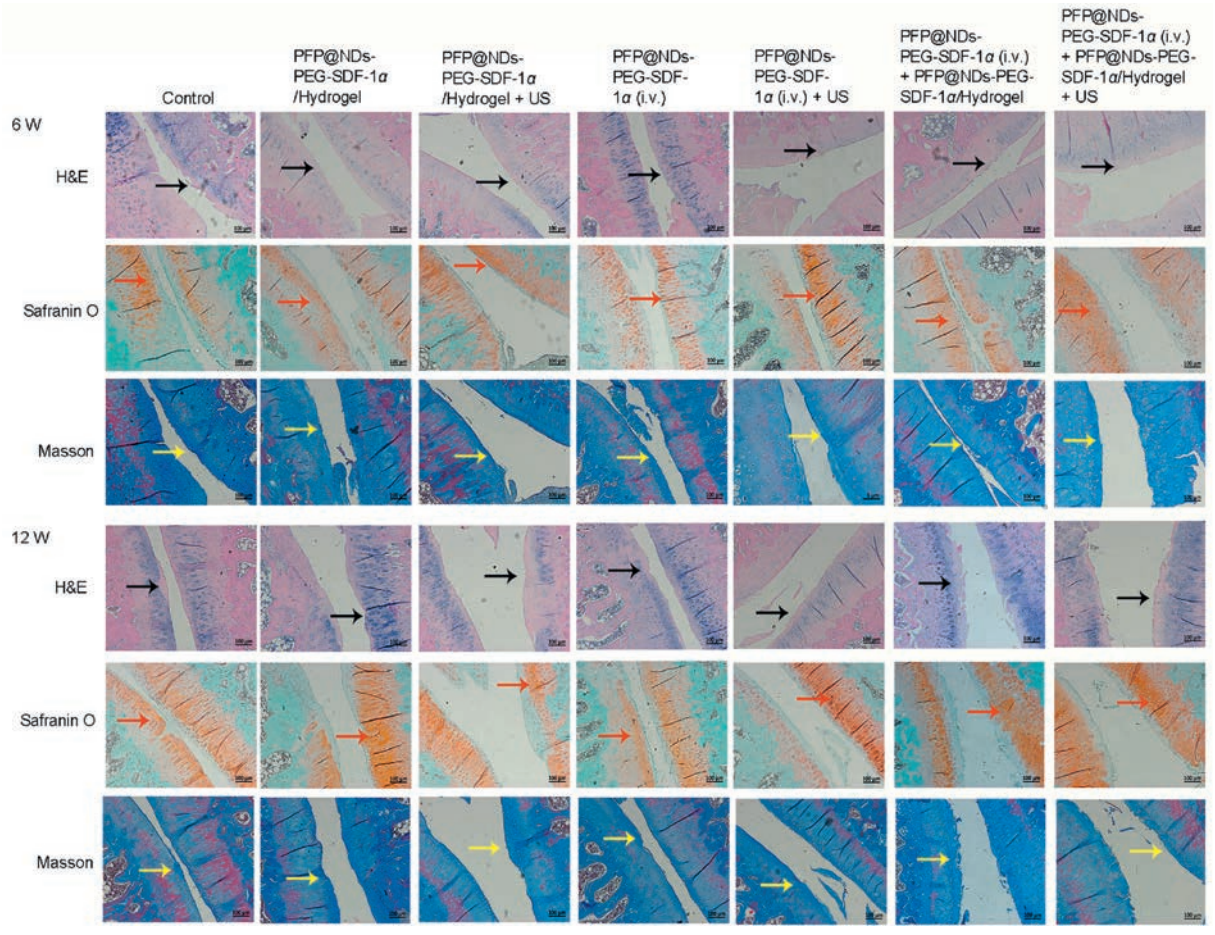


**Fig. 3.** Microscopy images of knee joints, histopathology tissues were stained with H&E, SO/FG, and Masson's trichrome 6 and 12 weeks after OA treatment.

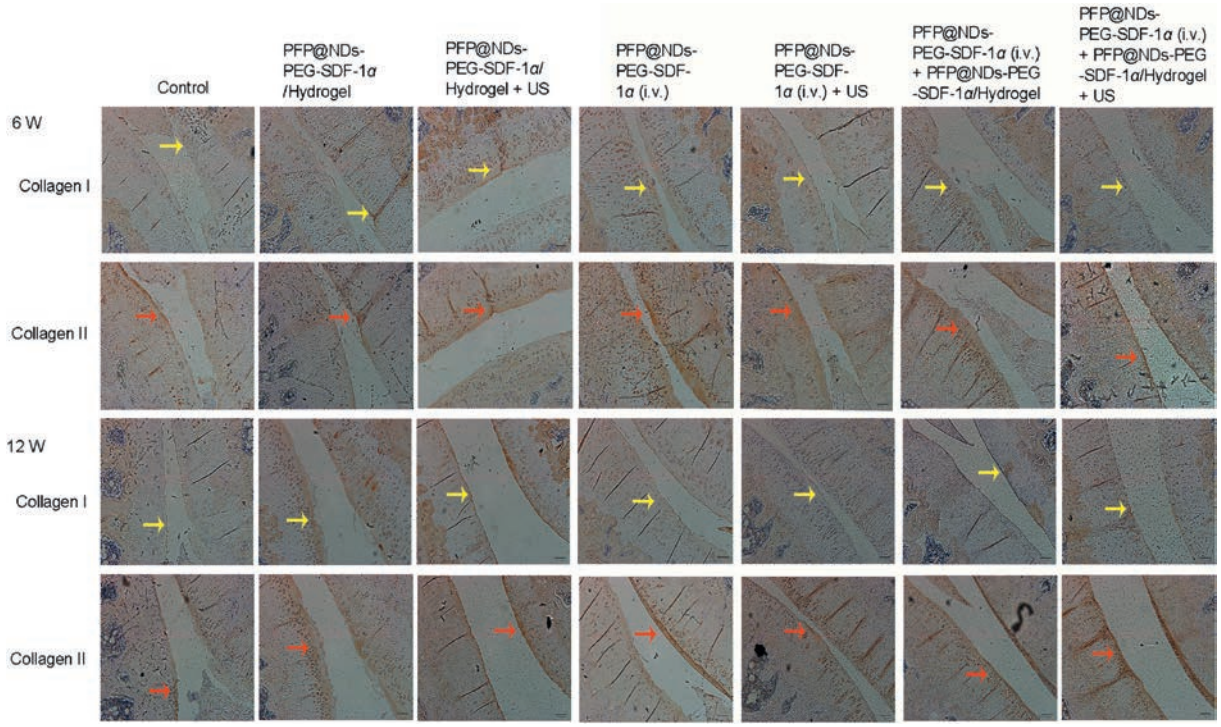


**Fig. 4.** Immunohistochemical detection of type I and type II collagen expression 6 and 12 weeks after OA treatment.

(i.v.) + PFP@NDs-PEG-SDF-1$\alpha$/hydrogel + US group is increased most significantly that the type II collagen content is higher than that in any of the other groups. And type I collagen level in this group is less than that in the other groups. However, more type I collagen and less type II collagen are produced in the control group and the PFP@NDs-PEG-SDF-1$\alpha$ (i.v.) group. Hyaline cartilage contains a large amount of type II collagen, therefore, the increase of type II collagen content is conducive to effective cartilage defect repair.

These results may be related to BMSCs affecting local endogenous progenitor cells through paracrine signaling, thereby initiating regeneration and repair [46], since BMSCs secrete multiple bioactive molecules, including cytokines, growth factors, and chemokines. The secretion of these agents by BMSCs is considered one of the most biologically significant functions of these cells under injury conditions [47], which can inhibit the local immune system *via* TNF-$\alpha$ and IL-1$\beta$, and stimulate mitosis and differentiation of inherent tissue repair cells or stem cells. BMSCs can also improve cartilage thickness and subchondral bone structure, which is consistent with the literature [48]. As previously reported, it is believed that SDF-1$\alpha$ not only enhances the migration of endogenous BMSCs [49], but also changes the characteristics of BMSCs, which can be beneficial for the repair of bone and cartilage [44] and can downregulate the expression of pro-inflammatory cyclooxygenase-2, pro-inflammatory interleukin, and collagenase in TNF$\alpha$-induced OA chondrocytes. The anti-inflammatory effect of bone marrow mesenchymal stem cell-derived extracellular vesicles (BMMSC-EVs) is related to the inhibition of NF-$\kappa$B signal transduction with NF-$\kappa$B activation being pivotal to OA pathology. OA chondrocytes treated with BMMSC-EVs are able to induce proteoglycan and type II collagen production, promote proliferation of these cells, and further promote cartilage repair. A number of studies have shown that promoting endogenous BMSCs homing in OA joints is beneficial to articular cartilage repair.

In summary, we successfully prepared PFP@NDs-PEG-SDF-1$\alpha$ nanodroplets, injectable thermosensitive chitosan hydrogels, and injectable chemotaxis hydrogel with good stability. The diameter of the nanodroplets was approximately 300 nm. The injectable thermosensitive chitosan hydrogel had a rapid gelation time and good elastic modulus, which could be used as a scaffold for homing stem cell attachment, providing a good extracellular microenvironment to cells. Combined with ultrasound, the injectable chemotaxis hydrogel allowed SDF-1$\alpha$ to enter cells or interstitial space through the cavitation effect and promoted additional stem cell homing. Ultrasound augmenting injectable chemotaxis hydrogel had a positive effect on the repair of OA articular cartilage. Overall, our results suggest that the treatment strategy of ultrasound augmenting injectable chemotaxis hydrogel has a bright prospect when it is applied in OA articular cartilage repair, *etc.* biomedical field.

## Declaration of competing interest

The authors declare that they have no known competing financial interests or personal relationships that could have appeared to influence the work reported in this paper.

## Acknowledgments

This work was financially sponsored by the National Natural Science Foundation of China (Nos. 81971622, 81671696, 82071938, and 51703141), Sichuan Science and Technology Program (Nos. 2019YFS0219, 2020YFH0087, and 2020YJ0055), the Post-Doctor Research Project, West China Hospital, Sichuan University (No. 2018HXBH077). We thank the support of China Scholarship Council and Chunhui Program of the Ministry of Education. We also thank our laboratory members for their generous help and gratefully acknowledge the help of Dr. Mi Zhou and Dr. Chao He for the analytical support and Ms. Xijing Yang, Ms. Ying Tian, and Ms. Zhen Yang of the Animal Experimental Center, West China Hospital, Sichuan University for the animal experiment. We also thank the support of Zhongkebaice Technology Service Co., Ltd., Beijing, China. We gratefully acknowledge the help of Ms. Li Li from the Laboratory of Pathology for histological support. We appreciate

Ms. Hui Wang from the Analytical & Testing Center of Sichuan University for the SEM characterization.

## Appendix A. Supplementary data

Supplementary material related to this article can be found, in the online version, at doi:https://doi.org/10.1016/j.cclet.2020.12.004.

## References

[1] J.A. Mcintyre, I.A. Jones, B. Han, C.T. Vangsness, Am. J. Sports Med. 46 (2018) 3550–3563.
[2] A. Goldberg, K. Mitchell, J. Soans, L. Kim, R. Zaidi, J. Orthop, Surg. Res. 12 (2017) 39.
[3] C.H. Jo, Y.G. Lee, W.H. Shin, et al., Stem Cells 32 (2014) 1254–1266.
[4] W. Wei, J. Luo, Hum. Gene Ther. 30 (2018) 119–126.
[5] M. Shariatzadeh, J. Song, S.L. Wilson, Cell Tissue Res. 378 (2019) 399–410.
[6] M.L. Vainieri, A. Lolli, N. Kops, et al., Acta Biomater. 101 (2020) 293–303.
[7] D.O. Visscher, E.J. Bos, M. Peeters, et al., Tissue Engineering C: Methods 22 (2016) 573–584.
[8] S.P. Nukavarapu, D.L. Dorcemus, Biotechnol. Adv. 31 (2013) 706–721.
[9] D. Goyal, S. Keyhani, E.H. Lee, J.H.P. Hui, Arthroscopy 29 (2013) 1579–1588.
[10] C.W. Ha, Y.B. Park, S.H. Kim, H.J. Lee, Arthroscopy 35 (2019) 277–288.
[11] M.K. Mamidi, A.K. Das, Z. Zakaria, R. Bhonde, Osteoarthr. Cartil. 24 (2016) 1307–1316.
[12] W.K. Aicher, H. Buhring, M.L. Hart, et al., Adv. Drug Del. Rev. 63 (2011) 342–351.
[13] K.B.L. Lee, V.T.Z. Wang, C. Yiong Huak, J.H.P. Hui, Ann Acad Med Singapore 41 (2012) 511–517.
[14] H. Nejadnik, J.H.P. Hui, E.P.F. Choong, B.C. Tai, E.H. Lee, Am. J. Sports Med. 38 (2010) 1110–1116.
[15] J. Huang, L. Chen, Z. Gu, J. Wu, Nanotechnol 15 (2019) 1357–1370.
[16] J. Huang, L. Chen, Q. Yuan, Z. Gu, J. Wu, J. Biomed. Nanotechnol. 15 (2019) 1371–1383.
[17] Y. Niu, T. Yang, R. Ke, C. Wang, Mater. Express 9 (2019) 563–569.
[18] J. Wu, Y. Qu, K. Shi, et al., Chin. Chem. Lett. 29 (2018) 1819–1823.
[19] B. Balakrishnan, R. Banerjee, Chem. Rev. 111 (2011) 4453–4474.
[20] Q.Q. Dou, S.S. Liow, E. Ye, R. Lakshminarayanan, X.J. Loh, Adv. Healthc. Mater. 3 (2014) 977.
[21] X.Q. Deng, N.N. Chao, W. Ding, et al., J. Biomed. Nanotechnol. 15 (2019) 756–768.
[22] K. Pariksha, C. Yahya, K. Pierre, et al., Molecules 21 (2016) 1580.
[23] X. Feng, X. Lu, D. Huang, et al., Cell. Mol. Neurobiol. 34 (2014) 859–870.
[24] T. Maerz, M.M. Fleischer, M.D. Newton, et al., Osteoarthr. Cartil. 25 (2017) 1335–1344.
[25] W. Yu, M. Shevtsov, X. Chen, H. Gao, Chin. Chem. Lett. 31 (2020) 1366–1374.
[26] S. Zhang, X. Pei, H. Gao, S. Chen, J. Wang, Chin. Chem. Lett. 31 (2020) 1060–1070.
[27] C. Yang, M. Zhou, C. He, et al., Nano-Micro Lett. 11 (2019) 87.
[28] L.N. Zamproni, M.V. Mundim, M.A. Porcionatto, A. des Rieux, Int. J. Pharm. 519 (2017) 323–331.
[29] Z. Shi, Q. Li, L. Mei, Chin. Chem. Lett. 31 (2020) 1345–1356.
[30] J. Wang, L. Fang, P. Li, et al., Nano-Micro Lett. 11 (2019) 74.
[31] X. Wang, J. Sheng, M. Yang, Chin. Chem. Lett. 30 (2019) 533–540.
[32] J. Liu, H. Qiu, Chin. Chem. Lett. 30 (2019) 1545–1546.
[33] E.G. Lima, K.M. Durney, S.R. Sirsi, et al., Acta Biomater. 8 (2012) 4334–4341.
[34] B.H. Zhu, L.Y. Wang, J.B. Huang, et al., J. Mater. Chem. B: Mater. Biol. Med. 7 (2019) 4581–4591.
[35] F. Mirahmadi, M. Tafazzolishadpour, M.A. Shokrgozar, S. Bonakdar, Mater. Sci. Eng. C 33 (2013) 4786–4794.
[36] A. Deng, X. Kang, J. Zhang, Y. Yang, S. Yang, Mater. Sci. Eng. C 78 (2017) 1147–1154.
[37] G. Adriana, L.A. Joanna, H. Wojciech, N. Maria, Colloids Surf. B: Biointerfaces 170 (2018) 152.
[38] H. Xu, E.M. Bouta, R.W. Wood, et al., Bone Res. 5 (2017) 1–7.
[39] N. Rapoport, Phase-shift, Nanomed. Nanobiotechnol. 4 (2012) 492–510.
[40] H. Maeda, T. Sawa, T. Konno, J. Control. Release 74 (2001) 47–61.
[41] N. Güvener, L. Appold, F. de Lorenzi, et al., Methods 130 (2017) 4–13.
[42] R. Niranjan, C. Koushik, S. Saravanan, et al., Int. J. Biol. Macromol. 54 (2013) 24–29.
[43] K.P.H. Pritzker, S. Gay, S.A. Jimenez, et al., Osteoarthr. Cartil. 14 (2006) 13–29.
[44] L.A. Vonk, S.F.J. van Dooremalen, N. Liv, et al., Theranostics 8 (2018) 906–920.
[45] M. Demoor, D. Ollitrault, T. Gomezleduc, et al., Biochim. Biophys. Acta 1840 (2014) 2414–2440.
[46] A.I. Caplan, J.E. Dennis, J. Cell. Biochem. 98 (2006) 1076–1084.
[47] J.I. Wolfstadt, B.J. Cole, D.J. Ogilvie-Harris, S. Viswanathan, J. Chahal, Sports Health 7 (2015) 38–44.
[48] L. Lu, X. Zhang, M. Zhang, et al., J. Dent. Res. 94 (2015) 1601–1609.
[49] P. Chen, J. Tao, S. Zhu, et al., Biomaterials 39 (2015) 114–123.